Neuroscience 322 (2016) 66–77

IMAGING MASS SPECTROMETRY DETECTS DYNAMIC CHANGES OF PHOSPHATIDYLCHOLINE IN RAT HIPPOCAMPAL CA1 AFTER TRANSIENT GLOBAL ISCHEMIA

S. MIYAWAKI,[a] H. IMAI,[a]* T. HAYASAKA,[b] N. MASAKI,[c] H. ONO,[a] T. OCHI,[a] A. ITO,[d] H. NAKATOMI,[a] M. SETOU[c] AND N. SAITO[a]

[a] *Department of Neurosurgery, Faculty of Medicine, The University of Tokyo, Tokyo, Japan*

[b] *Health Innovation & Technology Center, Faculty of Health Sciences, Hokkaido University, Sapporo, Hokkaido, Japan*

[c] *Department of Cell Biology and Anatomy, Hamamatsu University School of Medicine, Hamamatsu, Shizuoka, Japan*

[d] *Department of Neurosurgery, Teikyo University School of Medicine, Tokyo, Japan*

Abstract—*Background and purpose:* The initial steps in the cascade leading to cell death are still unknown because of the limitations of the existing methodology, strategy, and modalities used. *Methods:* Imaging mass spectrometry (IMS) was used to measure dynamic molecular changes of phosphatidylcholine (PC) species in the rat hippocampus after transient global ischemia (TGI) for 6 min. Fresh frozen sections were obtained after euthanizing the rats on Days 1, 2, 4, 7, 10, 14, and 21. Histopathology and IMS of adjacent sections compared morphological and molecular changes, respectively. *Results:* Histopathological changes were absent immediately after TGI (at Day 1, superacute phase). At Days 2–21 after TGI (from subacute to chronic phases), histopathology revealed neuronal death associated with gliosis, inflammation, and accumulation of activated microglia in CA1. IMS detected significant molecular changes after TGI in the same CA1 domain: increase of PC (diacyl-16:0/22:6) in the superacute phase and increase of PC (diacyl-16:0/18:1) in the subacute to chronic phases. *Conclusions:* Histopathology and IMS can provide comprehensive and complementary information on cell death mechanisms in the hippocampal CA1 after global ischemia. IMS provided novel data on molecular changes in phospholipids immediately after TGI. Increased level of PC (diacyl-16:0/22:6) in the pyramidal cell layer of hippocampal CA1 prior to the histopathological change may represent an early step in delayed neuronal death mechanisms.

Key words: hippocampus, imaging mass spectrometry, delayed neuronal cell death, phosphatidylcholine.

INTRODUCTION

The brain is intrinsically more vulnerable to ischemia than any other organ, and suffers significant damage after only a few minutes of cerebral blood flow deprivation. The actual mechanism causing damage to the brain, particularly the neurons, still remains to be elucidated. The hippocampus is recognized to be one of the most vulnerable neuroanatomical regions to the effects of ischemia (Schmidt-Kastner and Freund, 1991; Blanco-Suarez et al., 2014). Consequently, transient global ischemia (TGI) resulting in "delayed neuronal death" in the CA1 domain of the hippocampus has been widely used to investigate selective vulnerability (Kirino, 1982; Pulsinelli et al., 1982). A number of hypotheses have been proposed to explain the mechanisms of cell death, including continuous neuronal agitation after ischemia (Suzuki et al., 1983), mitochondrial damage (Abe et al., 1995), anomalies in Ca^{2+} homeostasis (Andine et al., 1988), anomalies in the regulatory mechanisms of glutamate concentration (Andine et al., 1988), and insufficient proteasome activity (Asai et al., 2002). However, the initial steps in the cascade leading to cell death are still unknown because of the limitations of the existing methodology, strategy, and modalities used.

Lipids, particularly phospholipids, are important for cellular function due to their structural functions in cellular membranes and their functions as precursors for various signaling pathways. Phospholipids, which are known for their high concentration in the brain, have important functions both during normal neuronal activity as well as during pathological processes (Adibhatla et al., 2006). Neuronal membrane phospholipids are affected by oxidative stress caused by ischemic injury. Up to now, there have been numerous studies attempting to identify key phospholipid components that could show changes during ischemia and play a critical role for cell death, to elucidate the mechanism of ischemic vulnerability of neuronal cell and to develop effective approach to prevent brain from ischemic injury (Goto et al., 1988).

*Corresponding author. Address: Department of Neurosurgery, Faculty of Medicine, The University of Tokyo, 7-3-1 Hongo, Bunkyo-ku, Tokyo 113-8655, Japan. Tel: +81-3-5800-8853; fax: +81-3-5800-8655.
E-mail address: hiimai-nsu@umin.ac.jp (H. Imai).

Abbreviations: AA, arachidonic acid; DHA, docosahexaenoic acid; ED1, ectodermal dysplasia 1; GFAP, glial fibrillary acidic protein; IMS, imaging mass spectrometry; MALDI, matrix-assisted laser desorption/ionization; NeuN, neuronal nuclei; PC, phosphatidylcholine; RT, room temperature; TBS/T, Tris-buffered saline with 0.5% Tween; TGI, transient global ischemia.

http://dx.doi.org/10.1016/j.neuroscience.2016.02.013
0306-4522/

The involvement of phospholipids in selective vulnerability of hippocampal CA1 has also been suggested (Kubota et al., 2001). However, because of their diverse and complex structure, there has been more difficulty for precise cellular phospholipid analyses compared with protein or peptide analyses.

Recently, ‘‘Omics” technology has been used in combination with conventional methodology to investigate the early stages of the pathways leading to cell death (Aebersold and Mann, 2003). Recent technical innovations in mass spectrometry have been applied to detect, analyze, and evaluate comprehensive data on dynamic changes in biological molecules such as proteins and lipids (Fenn et al., 1989; James et al., 2012). Imaging mass spectrometry (IMS) is a novel molecular imaging technique that enables comprehensive analysis of the spatial intensity distribution profiles of molecular species in biological tissue sections (Cornett et al., 2007; Gessel et al., 2014; Patterson et al., 2014).

The present study applied IMS to analyze the molecular kinetics of phospholipids in the hippocampus after TGI, as IMS analysis is best optimized for these molecules (Goto-Inoue et al., 2011; Jackson et al., 2014). The dynamic changes in phospholipids were profiled throughout the apoptotic process from Day 1 after TGI (the superacute phase) to Day 21 after TGI (the chronic phase) by correlating the findings of IMS with conventional histopathological evaluation of adjacent sections. The aim of this study was to track the initial features of ischemic neuronal cell death, reflected by changes in phospholipids as important cellular components, occurring prior to the morphological change detected by conventional histopathology. With this work, we propose new hypotheses to elucidate the mechanisms of vulnerability of neural cells to ischemic stress via a comprehensive discovery-based approach instead of the hypothesis-based approach.

EXPERIMENTAL PROCEDURES

Animals

Experiments were performed on male Sprague–Dawley rats (320–360 g; Charles River, Yokohama, Japan). One week before the surgery, the animals were housed under a 12-h light/dark cycle in a climate-controlled room with food and water available *ad libitum*. All efforts were made to minimize the number of animals used and their suffering. All experimental procedures were performed in accordance with the Animal Use Guidelines of The University of Tokyo, and approved by the Animal Care and Use Committee of The University of Tokyo (approved number P13-007) and Hamamatsu University School of Medicine.

Surgical procedure for global ischemia

The procedure for the induction of global ischemia in rats was reported previously (Kawahara et al., 2004). Briefly, 12 h before the induction of ischemia, each rat was anesthetized with 2.0% halothane in a mixture of 30% O_2 and 70% N_2 and the head secured in a stereotactic frame. Under the operating microscope, the first vertebral foramina were drilled through to locate the vertebral arteries which were exposed bilaterally, coagulated, and cut completely. The animals were then fasted overnight. After 12 h, the animals were anesthetized with 4% halothane in a mixture of 30% O_2 and 70% N_2, intubated and maintained under mechanical ventilation (2.0 mL 100 cycles/min, 1.5% isoflurane in a mixture of 30% O_2 and 70% N_2O). The partial pressures of arterial O_2 and CO_2 were maintained within the normal ranges throughout the surgery, and the rectal and temporal temperatures were maintained at 37.5 ± 0.2 °C with a heating pad and a heat lamp, respectively. Cerebral ischemia was induced for 6 min by occluding both common carotid arteries with aneurysm clips. The reproducibility of the global ischemia was further ensured by maintaining the mean blood pressure at 50 mmHg during occlusion by withdrawing blood from the right femoral artery and monitoring the blood pressure through a cannula in the left femoral artery. The clips were then removed to restore cerebral blood flow and anesthesia withdrawn. After regaining spontaneous respiration, the rats were extubated and returned to their cages. Sham control rats were treated similarly, except for the vertebral artery coagulation and carotid artery clipping procedures.

Preparation of tissue samples

The rats were euthanized on Days 1, 2, 4, 7, 10, 14, and 21 ($n = 3$ per time point) under 4% deep halothane anesthesia and then decapitated. The brains were rapidly removed, frozen in powdered dry ice, and stored at −80 °C. Coronal cryostat sections (10 μm) containing the hippocampus at the level of approximately 3.3 mm caudal from the bregma were placed onto normal glass slides and stored at −80 °C for immunohistochemistry, or placed onto glass slides coated with indium tin oxide (Bruker Daltonics, Bremen, Germany) and stored at −20 °C until matrix application and subsequent IMS analysis.

Immunohistochemistry

Rat brain sections on ordinary glass slides were warmed to room temperature (RT) and then air dried with a dryer for 20 min. After circling with a PAP pen, the sections were fixed with 4% paraformaldehyde/phosphate-buffered saline for 20 min at RT. The sections were stained with hematoxylin–eosin or cresyl violet, or immunostained for other markers. For immunohistochemical studies, the sections were rinsed well three times in Tris-buffered saline with 0.5% Tween (TBS/T) for 3 min. After blocking with 5% normal donkey serum in TBS/T at RT for 1 h, the sections were incubated overnight at 4 °C with the following primary antibodies: anti-neuronal nuclei (NeuN) antibody (1:500; Chemicon Mouse IgG MAB377, Millipore Corporation, Billerica, MA, USA) for neuronal cells, anti-ectodermal dysplasia 1 (ED1) antibody (1:300; AbD Setotec Mouse IgG MCA341R, Raleigh, NC, USA) for activated microglia, and anti-glial fibrillary acidic protein (GFAP) antibody (1:2000; Abcam Rabbit IgG 7260, Cambridge, United Kingdom) for activated

astrocytes. The sections were then rinsed well in TBS/T and incubated for 1 h at RT with appropriate secondary antibodies conjugated with Alexa 488, 546 (1:200; Molecular Probes, Eugene, OR, USA) for immunofluorescent staining for NeuN and GFAP, or with an appropriate biotinylated secondary antibody for the avi din–biotin–peroxidase complex method and diaminobenzidine detection for ED1. The numbers of NeuN-positive cells, GFAP-positive cells, and ED1-positive cells were counted in microscopic fields for an area of 500×750 μm ($0.375\ mm^2$) in the hippocampal CA1 domain, covering the stratum radiatum, pyramidal cell layer, and stratum oriens. Three coronal sections per animal at levels approximately 2.8/3.3/3.8 mm caudal from the bregma were collected and averaged.

IMS analysis

Rat brain sections on indium tin oxide-coated glass slides were attached to a special holder and inserted into a mass microscope (Shimadzu, Kyoto, Japan). The mass spectrometer is equipped with a matrix-assisted laser desorption/ionization (MALDI) chamber, a quadrupole ion trap, and a time of flight instrument. The objective lens enables observation of the sample in the MALDI chamber at high resolution (magnification: ×1.25, ×2.5, ×5, ×10, ×20, and ×40; Olympus, Tokyo, Japan). After obtaining an optical image and determining the measurement area for IMS analysis, the special holder was ejected from the mass microscope to coat the 2,5-dihydroxybenzoic acid matrix. A thin matrix layer was homogeneously applied onto the surface with a matrix sublimation instrument (Shimadzu) according to the following steps described later. Approximately 200 mg of 2,5-dihydroxybenzoic acid was placed in a tungsten boat at the bottom of the instrument chamber. The chamber was evacuated to a pressure of 10–20 Pa, and the tungsten boat was heated to 170 °C for 3 min. The special holder was then re-inserted into the mass microscope. IMS analysis was performed with a Nd/YAG laser running at 400 Hz, and mass spectra were obtained from 80 laser shots per measurement point in the range of m/z 700–900 in positive-ion mode. The spatial resolution (raster-scan pitch) was 15 μm per pixel. Laser energy was optimized to maximize the sensitivity of the signal detection in IMS analysis. The IMS dataset acquired by the mass microscope was converted to the ANALYZE 7.5 format file using special converter software (Shimadzu). The IMS data were statistically analyzed with SIMtool software (Shimadzu). Signal intensity was represented for each phosphatidylcholine (PC) species as relative intensity to the internal control in each slice. PC (diacyl-18:0/18:1) was used as the internal control, which was most abundant in corpus callosum and showed no histopathological changes through the time course after ischemia in our model (Kawahara et al., 2004). The abundance of PC (diacyl-18:0/18:1) in the corpus callosum was reported in a previous study (Sugiura et al., 2009).

The signal intensity of each PC species was used to assess the correlation to the histopathological cell counts at a next stage.

Abbreviations for glycerophospholipids

The structures of the side chains of glycerophospholipid species with one or two radial side chains are indicated within parentheses in the "head group (coupling scheme-sn1/sn2)" format [e.g., PC (diacyl-16:0/18:1)].

Statistical analysis

All data are expressed as mean ± standard deviation. Statistical analysis was conducted by a one-way analysis of variance for the cell count and relative intensity of the mass spectrum for comparing more than two groups, followed by the post hoc Bonferroni–Dunn test. Student's t-test was used for comparing two groups. Spearman's Rank Correlation test was applied to evaluate the correlation between PC signal intensity and histopathological cell count across all sampled experimental animals. Differences were considered significant at $P < 0.05$.

RESULTS

Histopathology

Hematoxylin–eosin and cresyl violet staining. Normal morphological features with intact, round neuronal cell bodies were found in the pyramidal cell layers of the hippocampus and dentate gyrus in the sham controls. Similarly, no morphological abnormality was found in the hippocampal pyramidal cells and dentate gyrus of rats sacrificed on Day 1 after global ischemia (Fig. 1). This phase from the onset of ischemia to the end of Day 1 is called the *superacute* phase in this study. Abnormal morphological features were observed in some pyramidal neurons in the hippocampal CA1 on Day 2 after ischemia: shrinkage and triangulation of nucleus and cytoplasm, and increased eosinophilia of cytoplasm (data not shown). These characteristic features of ischemic damage became more apparent on Day 4 (data not shown). Degenerative morphological changes, characteristic of cell death, were observed in most pyramidal cells of the hippocampal CA1 on Day 7. This phase from Days 2 to 7 was called the *subacute* phase in this study. Next the pyramidal cells of the hippocampal CA1 had been replaced by numerous cells of unknown origin, morphologically resembling inflammatory cells, by Day 21. This phase was called the *chronic* phase in this study.

Immunohistochemistry

NeuN-immunoreactive neurons. The numbers of NeuN-immunoreactive cells in the pyramidal cell layer in the hippocampus and dentate gyrus were approximately the same in both the sham controls and the experimental rats on Day 1 after ischemia (Fig. 2A). The numbers of NeuN-immunoreactive cells began to decline gradually on Day 2 (data not shown), and most NeuN-immunoreactive cells in the hippocampal CA1 disappeared by Day 7 in the subacute phase.

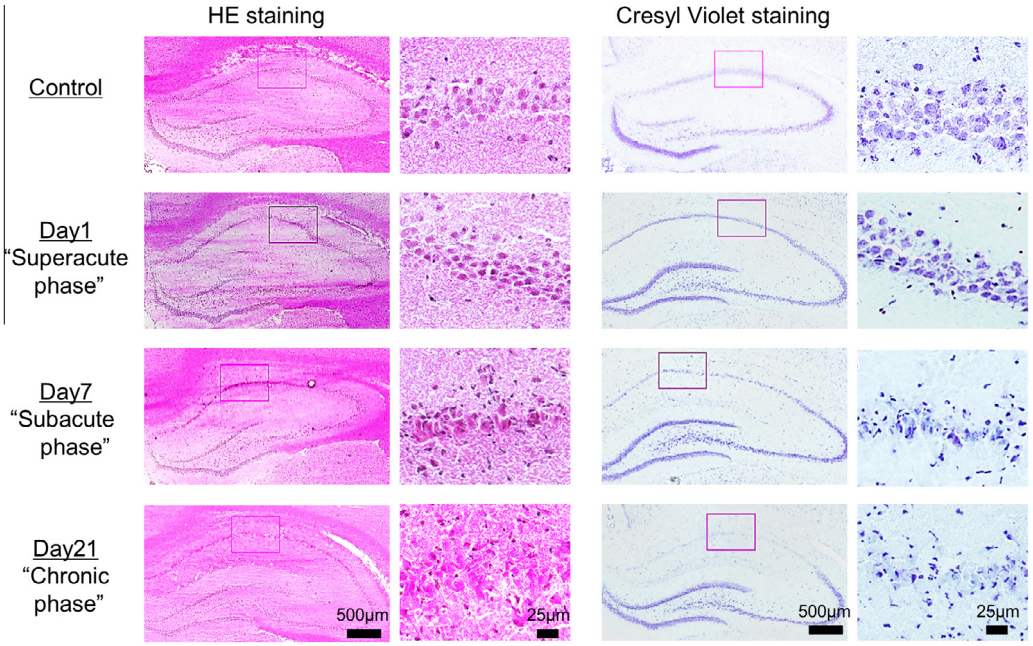

Fig. 1. Hematoxylin–eosin (HE) and cresyl violet staining of the rat hippocampus after transient global ischemia (TGI). In the sham controls, the pyramidal neuronal cells in the hippocampus and dentate gyrus had normal morphological features with intact, round neuronal cell bodies. On Day 1 after TGI (superacute phase), the hippocampal pyramidal cells and dentate gyrus had no morphological abnormalities, similar to the sham controls. On Day 7 (subacute phase), most pyramidal cells of the hippocampal CA1 showed degenerated morphological changes of cell death. On Day 21 (chronic phase), the pyramidal cells of hippocampal CA1 were replaced by numerous cells of unknown origin, morphologically resembling inflammatory cells.

NeuN-immunoreactive cells were almost undetectable on Day 21 in the chronic phase. The number of NeuN-immunoreactive cells in the hippocampal CA1 was similar in the superacute phase and in the sham controls (164.0 ± 25.0 vs 166.6 ± 16.0 cells/0.375 mm^2), but decreased significantly in the subacute phase compared to the sham controls (29.6 ± 10.3 vs 166.6 ± 16.0 cells/0.375 mm^2, $P < 0.001$), and decreased even more significantly in the chronic phase (5.6 ± 2.1 vs 166.6 ± 16.0 cells/0.375 mm^2, $P < 0.001$) (Fig. 2C). These results confirmed that the delayed neuronal cell death observed by conventional histopathology had begun in the subacute phase.

GFAP-immunoreactive astrocytes. GFAP-immunoreactive astrocytes maintained normal shapes with thin long processes in both sham control and superacute phase specimens (Fig. 2A). Apparent morphological changes appeared in the hippocampal CA1 in the subacute phase, such as typical hypertrophic astrocytes with thickened processes and enlarged cell bodies. The number of hypertrophic GFAP-immunoreactive astrocytes increased and gliosis progressed together with fewer NeuN-immunoreactive cells in the chronic phase. This number, however, was similar in the superacute phase and in the sham controls (192.3 ± 13.6 vs 201.6 ± 6.0 cells/0.375 mm^2) (Fig. 2D). The number of GFAP-immunoreactive cells increased significantly compared to the sham controls at later time points (Day 7) (255.3 ± 24.6 vs 201.6 ± 6.0 cells/0.375 mm^2, $P < 0.001$), and remained significantly higher in the chronic phase (273.3 ± 18.5 vs 201.6 ± 6.0 cells/0.375 mm^2, $P < 0.001$). These results showed that no morphological change occurred in the astrocytes in the superacute phase, but gliosis with hypertrophic GFAP-immunoreactive astrocytes became dominant in the hippocampal CA1 in the subacute phase and persisted until the chronic phase.

ED1-immunoreactive microglia. No ED1-immunoreactive microglia was observed in the hippocampal CA1 or dentate gyrus in the sham controls or in the superacute phase (Fig. 2B). ED1-immunoreactive microglial cells began to emerge on Day 2 (data not shown), and their number increased significantly on Day 7 predominantly in the pyramidal cell layer of the hippocampal CA1. ED1-immunoreactive microglia widely spread across the hippocampal CA1 in the chronic phase. ED1-immunoreactive cells were undetected in the hippocampal CA1 in the superacute phase and in the sham controls, but the number of cells increased significantly in the subacute phase compared to the sham controls (255.0 ± 22.9 vs 0 cells/0.375 mm^2, $P < 0.001$), and remained significantly higher in the chronic phase (232.6 ± 20.8 vs 0 cells/0.375 mm^2, $P < 0.001$) (Fig. 2E). These results confirmed that ED1-immunoreactive cells were absent in the superacute phase, dramatically proliferated in the subacute phase, and persisted until the chronic phase.

IMS analysis

Profiling of sham control hippocampus. The MALDI-IMS system was used in the positive ion detection mode

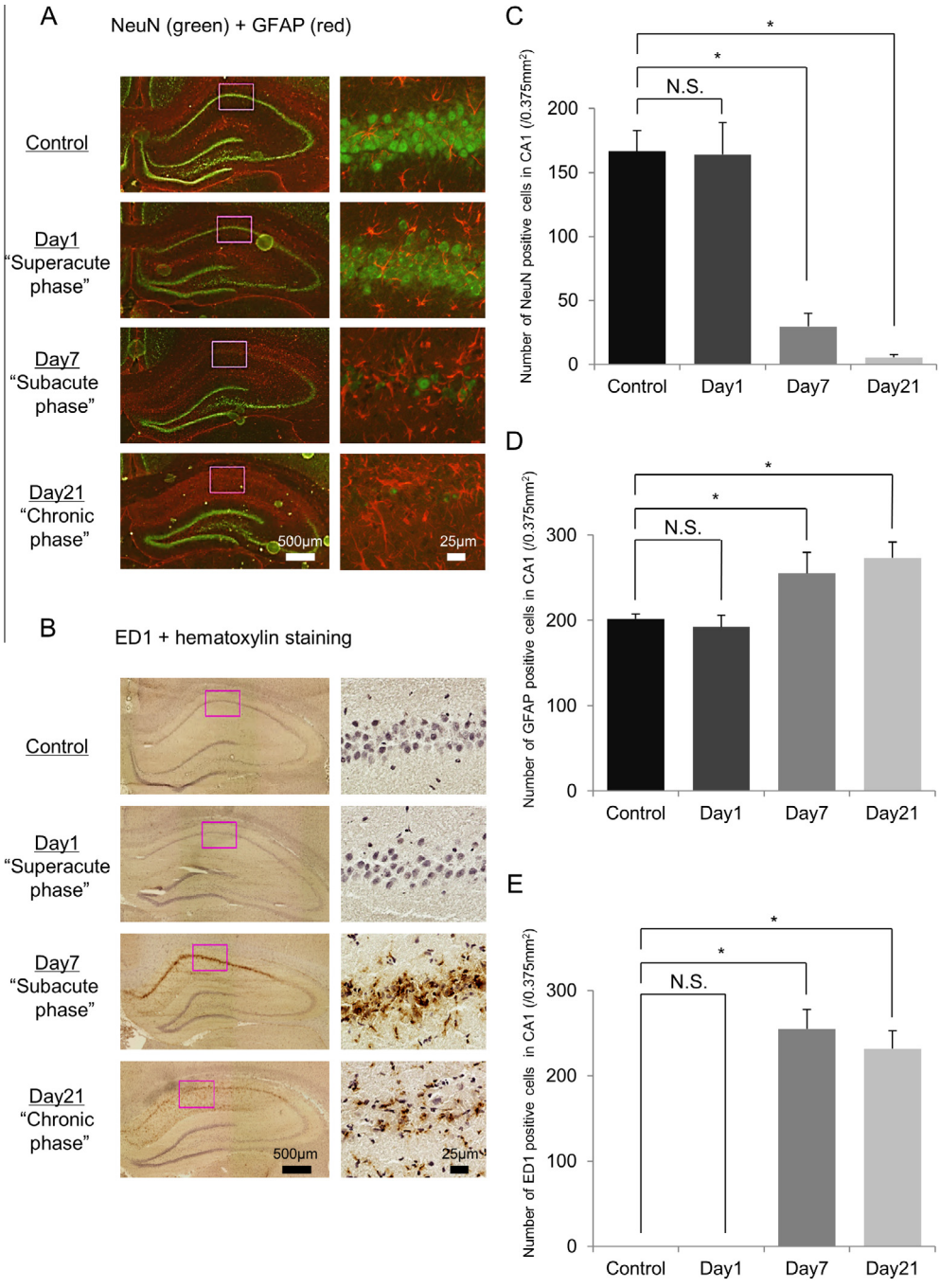

for the analysis of molecular changes in phospholipids in the hippocampus during the course of delayed neuronal cell death (from the superacute to the chronic phase). Approximately 150 peaks were detected in the mass range of 700 < *m*/*z* < 900 (Fig. 3A). Ten intense mass peaks were assigned to abundant PC species based on their molecular masses and previously reported data (Sugiura et al., 2009; Koizumi et al., 2010; Hanada et al., 2012), and the tissue distributions of these 10 major species in the hippocampus were visualized (Fig. 3B). IMS analysis of the hippocampus of the sham controls revealed characteristic PC distribution patterns dependent on fatty acid composition, which reflected the heterogeneous membrane lipid compositions of distinct cell types. For example, PC (diacyl-16:0/20:4) was evenly distributed across the entire hippocampus and dentate gyrus. On the other hand, PC (diacyl-16:0/18:1), which is the most abundant molecule in the hippocampus, and PC (diacyl-16:0/16:0) were also distributed across the entire hippocampus and dentate gyrus but were less dominant in the pyramidal cell layer of the hippocampus and granular cell layer of the dentate gyrus. PC (diacyl-18:0/18:1) was mainly distributed in the white matter, such as the corpus callosum, and less dominant in the hippocampus and gray matter. These results confirmed that IMS had adequate sensitivity to discriminate the

anatomical distribution of various PC species according to their molecular masses.

Profiling of the hippocampus in the superacute phase. No histological changes were observed in the superacute phase after TGI, but IMS showed increases in three PC species in the pyramidal cell layer: PC (diacyl-16:0/20:4), PC (diacyl-16:0/22:6), and PC (diacyl-18:0/20:4) (Fig. 4A). On the other hand, no changes were observed in three other PC species: PC (diacyl-16:0/16:0), PC (diacyl-18:0/18:1), and PC (diacyl-16:0/16:1) (Fig. 5). The PC species showing increases contained polyunsaturated fatty acids, such as docosahexaenoic acid (DHA) (22:6) and arachidonic acid (AA) (20:4) (Fig. 4A). The PC species which contained AA (20:4), PC (diacyl-16:0/20:4), and PC (diacyl-18:0/22:4) increased in the pyramidal cell layer of the hippocampal CA1, the pyramidal cell layer of the hippocampal CA3, and the granular cell layer of the dentate gyrus. In particular, PC (diacyl-16:0/22:6) was the only species to show a significantly greater increase specifically in the pyramidal cell layer of CA1. Semi-quantitative measurements showed that the signal intensity ratio of PC (diacyl-16:0/22:6) in the pyramidal cell layer of the CA1 was significantly higher in the superacute phase than in the sham controls (0.91 ± 0.05 vs 0.61 ± 0.02, $P < 0.001$) (Fig. 4B). These findings, together with the absence of morphological change, indicate that the changes in PC species reflect remodeling of the cell components rather than cell replacement.

Profiling of the hippocampus in the subacute phase. The histopathological study showed reduction of pyramidal cells in the hippocampal CA1 and replacement by ED1-immunoreactive microglial cells and gliosis (higher number of hypertrophic GFAP-immunoreactive astrocytes). In this cellular environment, only one PC species, PC (diacyl-16:0/18:1), specifically increased in that domain (Fig. 6A). The signal intensity ratio of PC (diacyl-16:0/18:1) in the hippocampal CA1 was significantly higher in the subacute phase than in the sham controls (3.03 ± 0.16 vs 1.87 ± 0.12, $^{*}P < 0.001$) (Fig. 6B). In contrast, three PC species, PC (diacyl-16:0/16:0), PC (diacyl-18:0/18:1), and PC (diacyl-16:0/16:1), showed no apparent changes in the subacute phase (Fig. 5). On the other hand, three PC species, PC (diacyl-16:0/20:4), PC (diacyl-16:0/22:6), and PC (diacyl-18:0/20:4), showed transient increase in the superacute phase and decrease to baseline level in the subacute phase (Fig. 4). These results indicate that the increase of PC (diacyl-16:0/18:1) in the hippocampal CA1 can be attributed to cellular replacement by microglia and hypertrophic astrocytes in the subacute phase (Fig. 2).

Profiling of hippocampus in the chronic phase. The histopathological study showed total loss of neuronal cells in the hippocampal CA1 and accumulation of ED1-immunoreactive microglial cells together with progress of gliosis (higher number of hypertrophic GFAP-immunoreactive astrocytes) in the chronic phase (Fig. 2). These findings indicate that replacement of neuronal cells in the hippocampal CA1 by other types of cells had begun in the subacute phase and was almost complete in the chronic phase (Fig. 2). PC (diacyl-16:0/18:1) significantly increased in the CA1 in this phase (Fig. 6A). On the other hand, three PC species, PC (diacyl-16:0/16:0), PC (diacyl-18:0/18:1), and PC (diacyl-16:0/16:1), showed no change as in the previous superacute and subacute phase (Fig. 5). The three PC species, PC (diacyl-16:0/20:4), PC (diacyl-16:0/22:6), and PC (diacyl-18:0/20:4), which showed transient increase in the superacute phase and decrease to baseline level in the subacute phase, also remained at the baseline in the chronic phase (Fig. 4A). The signal intensity ratio of PC (diacyl-16:0/18:1) in the hippocampal CA1 was significantly higher in the chronic phase than in the sham controls (3.23 ± 0.27 vs 1.87 ± 0.12, $^{*}P < 0.001$) (Fig. 6B). These results indicate that increase of PC (diacyl-16:0/18:1) in CA1 reflects the replacement of neuronal cells by

Fig. 2. Immunohistochemical analyses of the rat hippocampus after transient global ischemia. (A) Double staining with glial fibrillary acidic protein (GFAP) and neuronal nuclei (NeuN). In the sham controls, the pyramidal cell layer in the hippocampus and dentate gyrus apparently showed NeuN immunoreactivity. GFAP-immunoreactive astrocytes had normal shapes, with thin long processes. On Day 1 after ischemia (superacute phase), approximately the same numbers of NeuN-immunoreactive cells were present as in the sham controls. GFAP-immunoreactive astrocytes maintained normal shapes, with thin long processes. On Day 7 (subacute phase), most NeuN-positive cells of the hippocampal CA1 had disappeared. Apparent morphological changes had emerged in GFAP-immunoreactive astrocytes in the hippocampal CA1, such as typical hypertrophic astrocytes with thickened processes and enlarged cell bodies. On Day 21 (chronic phase), NeuN-immunoreactive cells had almost completely disappeared. The number of hypertrophic GFAP-immunoreactive astrocytes increased and gliosis progressed. (B) Ectodermal dysplasia 1 (ED1) staining with hematoxylin staining. No ED1-immunoreactive microglia was observed in the hippocampal CA1 or dentate gyrus in the sham controls and in the superacute phase. On Day 7 (subacute phase), the number of ED1-immunoreactive microglial cells increased significantly and predominantly accumulated in the pyramidal cell layer of the hippocampal CA1. In the chronic phase, ED1-immunoreactive microglial cells were distributed widely across the hippocampal CA1. (C) The number of NeuN-immunoreactive cells in the hippocampal CA1 was similar in the superacute phase ($n = 3$) and in the sham controls ($n = 3$) (164.0 ± 25.0 vs 166.6 ± 16.0 cells/0.375 mm^2), but had significantly decreased in the subacute phase ($n = 3$) (29.6 ± 10.3 vs 166.6 ± 16.0 cells/0.375 mm^2, $^{*}P < 0.001$) and in the chronic phase ($n = 3$) compared to the sham controls ($n = 3$) (5.6 ± 2.1 vs 166.6 ± 16.0 cells/0.375 mm^2, $^{*}P < 0.001$). (D) The number of GFAP-immunoreactive cells was similar in the superacute phase ($n = 3$) and in the sham controls ($n = 3$) (192.3 ± 13.6 vs 201.6 ± 6.0 cells/0.375 mm^2), but had significantly increased on Day 7 ($n = 3$) compared to the sham controls ($n = 3$) (255.3 ± 24.6 vs 201.6 ± 6.0 cells/0.375 mm^2, $^{*}P < 0.001$) and remained significantly higher in the chronic phase ($n = 3$) (273.3 ± 18.5 vs 201.6 ± 6.0 cells/0.375 mm^2, $^{*}P < 0.001$). (E) ED1-immunoreactive cells were undetected in the hippocampal CA1 in the superacute phase and in the sham controls. The number of ED1-immunoreactive cells increased significantly in the subacute phase ($n = 3$) compared to the sham controls ($n = 3$) (255.0 ± 22.9 vs 0 cells/0.375 mm^2, $^{*}P < 0.001$), and remained significantly higher in the chronic phase ($n = 3$) (232.6 ± 20.8 vs 0 cells/0.375 mm^2, $^{*}P < 0.001$). N.S., not significant.

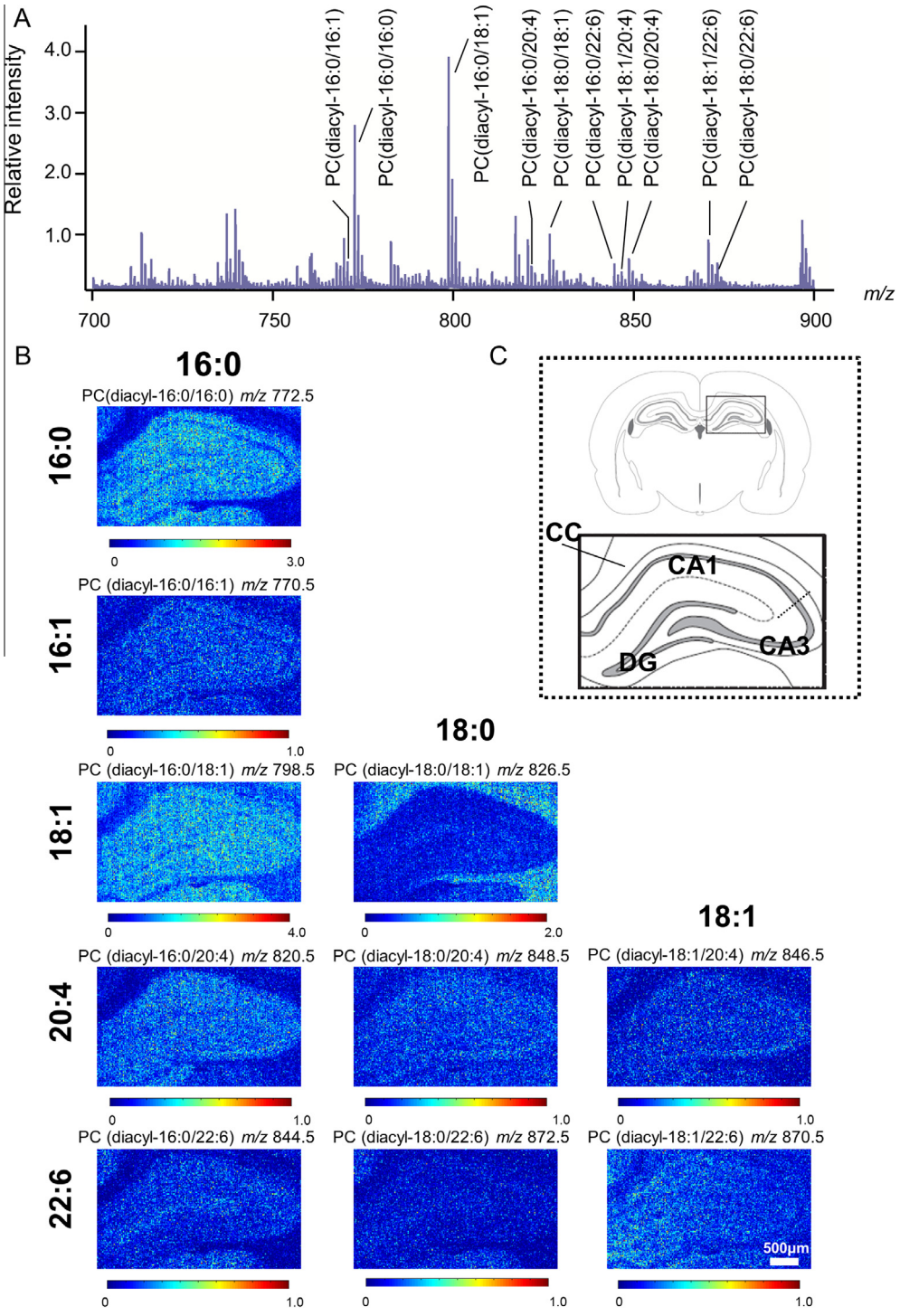

Fig. 3. (A) Representative matrix-assisted laser desorption/ionization mass spectrometry spectrum obtained from the rat hippocampal CA1 of the sham control. Intense mass peaks corresponding to 10 abundant phosphatidylcholines (PCs) were assigned based on their masses and previously reported data. (B) Differential distribution of PC species in the hippocampus of the sham controls. Imaging mass spectrometry (IMS) images of PCs are arranged according to their fatty acid (FA) compositions; PCs with identical FA compositions at the sn-1 position are arranged vertically, and PCs with identical FA compositions at the sn-2 position are arranged horizontally. The specific FA composition is associated with several unique localization features in the hippocampus. IMS analysis of the sham controls revealed characteristic PC distribution patterns dependent on FA composition, which reflected the heterogeneous membrane lipid compositions of distinct cell types. For example, PC (diacyl-16:0/20:4) was distributed across the entire hippocampus and dentate gyrus. On the other hand, PC (diacyl-16:0/18:1), which is the most abundant molecule in the hippocampus, and PC (diacyl-16:0/16:0) were also distributed across the entire hippocampus and dentate gyrus but were less dominant in the pyramidal cell layer of the hippocampus and granule cell layer of the dentate gyrus. PC (diacyl-18:0/18:1) was mainly distributed in the white matter, such as the corpus callosum, and less dominant in the hippocampus or gray matter. (C) Scheme of the rat brain section including the hippocampus. Scheme shows CA1 lesion, CA3 and dentate gyrus (DG) of the hippocampus and corpus callosum (CC). Scheme was quoted from ‘‘The rat brain in stereotaxic coordinates (6th edition)” (Paxinos and Watson, 2006) and partially modified with the permission of ELSEVIER.

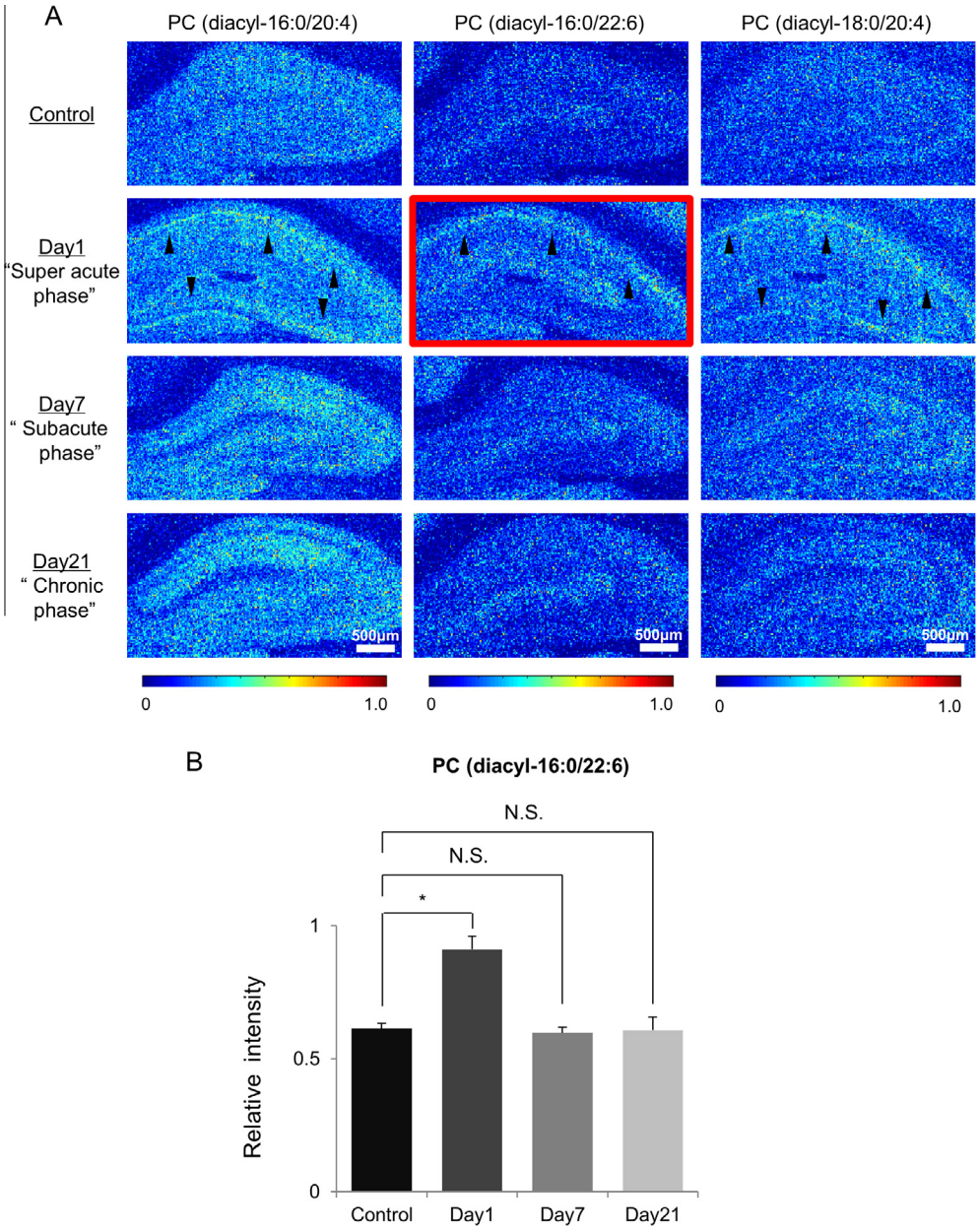

Fig. 4. (A) Imaging mass spectrometry analysis of phosphatidylcholine (PC) species which increased in the hippocampal CA1 in the superacute phase. Three PC species, PC (diacyl-16:0/20:4), PC (diacyl-16:0/22:6), and PC (diacyl-18:0/20:4), increased in the pyramidal cell layer during the superacute phase (arrowheads), when no histological changes had occurred ($n = 3$). These PC species contained polyunsaturated fatty acid, such as docosahexaenoic acid (22:6) and arachidonic acid (20:4). PC species which contained arachidonic acid (20:4), PC (diacyl-16:0/20:4), and PC (diacyl-18:0/20:4) increased in the pyramidal cell layer of the hippocampal CA1, the pyramidal cell layer of the hippocampal CA3, and the granule cell layer of the dentate gyrus. PC (diacyl-16:0/22:6) was the only species to show a significantly greater increase specifically in the pyramidal cell layer of the hippocampal CA1 ($n = 3$). (B) The signal intensity ratio of PC (diacyl-16:0/22:6) in the pyramidal cell layer of the hippocampal CA1 was significantly higher in the superacute phase ($n = 3$) than in the sham controls ($n = 3$) (0.91 ± 0.05 vs 0.61 ± 0.02, $^{*}P < 0.001$). However, the signal intensity ratio of PC (diacyl-16:0/22:6) in the pyramidal cell layer of the hippocampal CA1 in the subacute phase ($n = 3$) did not show significant difference compared to sham controls ($n = 3$) (0.59 ± 0.02 vs 0.61 ± 0.02) nor that in the chronic phase ($n = 3$) (0.60 ± 0.05 vs 0.61 ± 0.02).

ED1-immunoreactive microglial cells and hypertrophic GFAP-immunoreactive astrocytes in the chronic phase.

Correlation analysis between PC (diacyl-16:0/18:1) and cell count of GFAP-immunoreactive astrocyte

The signal intensity of PC (diacyl-16:0/18:1) and the cell count of GFAP-immunoreactive astrocyte had significant correlation (Spearman rank correlation coefficient $r = 0.85$, $p < 0.05$).

DISCUSSION

The present study used the TGI model to compare the molecular and histological features of delayed neuronal cell death. The TGI model rather than a focal ischemia model was used because the process of cell death after

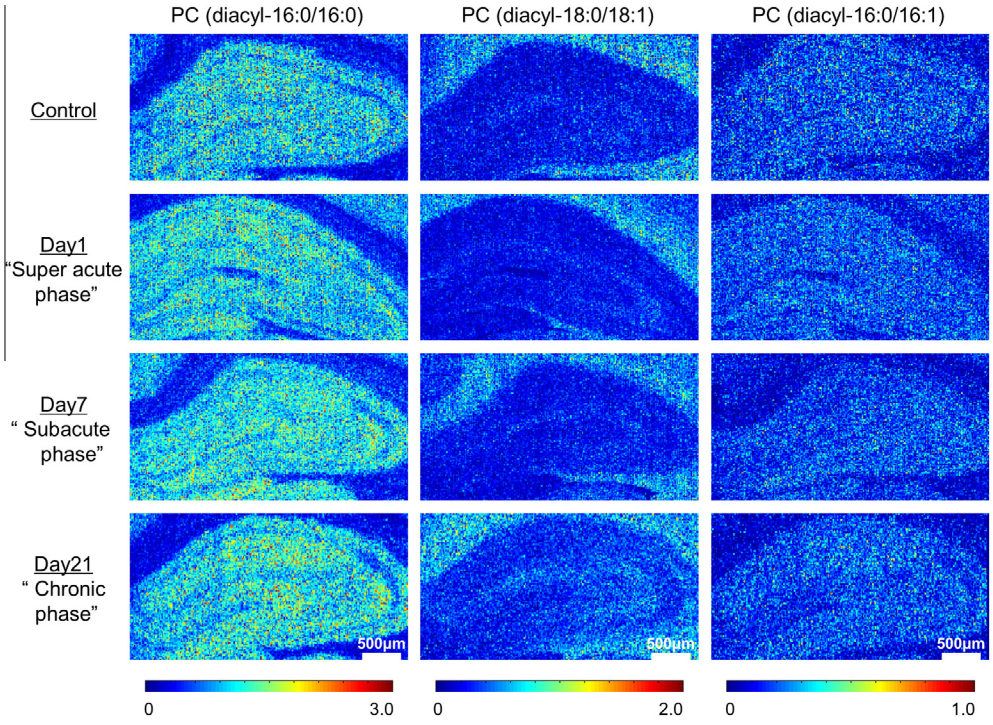

Fig. 5. Imaging mass spectrometry analysis of phosphatidylcholine (PC) species that showed no apparent change in the time course after transient global ischemia. Three PC species, PC (diacyl-16:0/16:0), PC (diacyl-18:0/18:1), and PC (diacyl-16:0/16:1), showed no apparent change in the superacute (n = 3), subacute (n = 3), or chronic phases (n = 3).

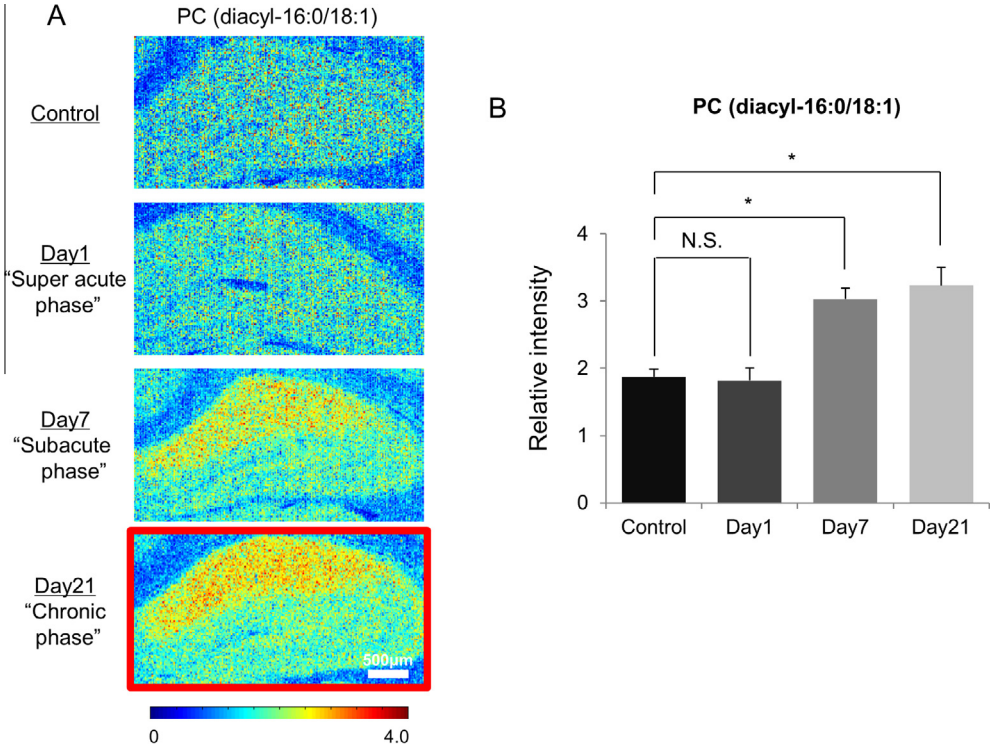

Fig. 6. (A) Imaging mass spectrometry analysis of phosphatidylcholine (PC) species showed increase in the hippocampal CA1 in the subacute phase and chronic phase. One PC species, PC (diacyl-16:0/18:1), increased in the hippocampal CA1 specifically in the subacute (n = 3) and chronic phases (n = 3). (B) The signal intensity ratio of PC (diacyl-16:0/18:1) in the hippocampal CA1 in the superacute phase (n = 3) did not show significant changes compared to that in sham controls (n = 3) (1.82 ± 0.18 vs 1.87 ± 0.12). However, the signal intensity ratio of PC (diacyl-16:0/18:1) in the hippocampal CA1 was significantly higher in the subacute phase than in the sham controls (3.03 ± 0.16 vs 1.87 ± 0.12, $^{*}P < 0.001$) and in the chronic phase (3.23 ± 0.27 vs 1.87 ± 0.12, $^{*}P < 0.001$).

focal ischemia (mainly necrosis) occurs within minutes compared to the slow progress of delayed neuronal cell death over days after global ischemia. Therefore, only the global ischemia model provides sufficient time for detailed IMS analysis (Kirino, 1982; Pulsinelli et al., 1982). The region of interest was limited to the hippocampal CA1 cell layer because this anatomical region is most vulnerable to ischemia and undergoes cell death with high reproducibility. Such reproducibility is critical, because IMS analysis focuses on morphologically intact cells which will finally undergo cell death. The animal model of TGI was developed by Kirino (1982), who discovered the phenomenon of delayed neuronal cell death in the gerbil. Since then, the gerbil forebrain ischemia model has been developed for research on delayed neuronal cell death, and various experimental studies have advanced our knowledge on stroke (Kawahara et al., 1998; Asai et al., 2002; Yonekura et al., 2006). Adding induced hypotension to 4-vessel occlusion in the rat model has further enhanced reproducibility, allowing the investigation of gene expression during the superacute phase of ischemia directly after global cerebral ischemia (Kawahara et al., 2004), as well as neuronal cell regeneration induced by activation of endogenous stem cells by administering growth factors to tissues after ischemic neuronal cell death (Nakatomi et al., 2002; Kawahara et al., 2004; Oya et al., 2009).

The present study extended from Days 1 to 21 after TGI. Thus, we could evaluate the molecular changes not only in the superacute phase after TGI but also in the subacute to chronic phases. The histopathological findings showed that activated microglial cells and reactive astrocytes replaced the neurons of the hippocampal CA1 during these last two phases. This period provided the most suitable conditions for IMS investigation since the apparent morphological changes should be reflected in the profile of the PC species due to the replacement of cells. Previous IMS findings using this ischemia model have revealed the molecular changes associated with tissue replacement in the chronic phase after ischemia (Koizumi et al., 2010; Hankin et al., 2011; Shanta et al., 2012; Wang et al., 2012). In the present study, IMS revealed that PC (diacyl-16:0/18:1) increased throughout the whole CA1 domain after TGI (Fig. 6). PC (diacyl-16:0/18:1) is a type of phospholipid which contains oleic acid (18:1), a monounsaturated fatty acid. Monounsaturated fatty acids have been reported to increase in reactive astrocytes, indicating the important role of monounsaturated fatty acid in gliotic change in the brain (Glynn, 2013). Moreover, monounsaturated fatty acids, including oleic acid (18:1), have been related to microglial activation (Button et al., 2014). These observations could be an explanation for our finding of increase in PC species including oleic acid (18:1) in hippocampal CA1 in the subacute to the chronic phases after TGI, where activated microglial cells and reactive astrocytes replaced the neurons. Therefore, PC (diacyl-16:0/18:1) is an important component and might be a biomarker of inflammatory change in the hippocampus. The significant correlation between the signal intensity of PC (diacyl-16:0/18:1) and the cell count of GFAP immunoreactive astrocytes supports our speculation about the association between PC (diacyl-16:0/18:1) and gliosis.

In this study, histopathology revealed no apparent morphological change in the hippocampal CA1 during the superacute phase (Day 1 after ischemia). However, the neuronal cells of the hippocampal CA1 are clearly destined to undergo cell death at this time point, as the CA1 neuronal cells should start remodeling from their normal state toward neuronal cell death after exposure to ischemia. Therefore, we suggest that detection of molecular changes in neuronal cells in the remodeling phase, or immediately after global cerebral ischemia, is equivalent to detecting the initiation of the molecular changes associated with programed neuronal cell death or apoptosis. In this study, IMS could detect the types of changes occurring in the remodeling phase at the level of metabolic molecules, which would not be possible by other modalities due to limitations in sensitivity.

The present study revealed that specific increase of PC (diacyl-16:0/22:6) occurs in the pyramidal cell layer of the hippocampal CA1 on Day 1 after ischemia (Fig. 4). Association of PC (diacyl-16:0/22:6) and foreplay processes involved in cell death is speculated by the fact that PC (diacyl-16:0/22:6) was the only PC species increased in the pyramidal cell layer of the hippocampal CA1 on Day 1 after ischemia. The absence of histopathological changes in the hippocampal CA1 on Day 1 after ischemia precluded the possibility of correlation analysis of signal intensity of PC (diacyl-16:0/22:6) and any quantitative cell changes in that area of interest.

There are several reports showing increase and decrease of specific phospholipids in the brain in neurodegenerative diseases, such as Alzheimer's disease, as a result of membrane degradation (Grimm et al., 2011). We believe that the increase of PC (diacyl-16:0/22:6) in the pyramidal cell layer of the hippocampal CA1 should be a result of membrane degradation consequent to ischemic stress.

Such increase in PC (diacyl-16:0/22:6) in the hippocampal CA1 might occur through several molecular mechanisms. For example, the compositional diversity of PCs is tightly regulated to maintain homeostasis under physiological conditions (Hermansson et al., 2011). The balance between synthesis and degradation is controlled by various enzymes, such as phospholipase A_2 and lysophospholipid acyltransferases (Sun et al., 2004; Shindou and Shimizu, 2009). Under pathological conditions, such as ischemia, the activities of these enzymes might change resulting in loss of physiological balance. Consequently, the increase of PC (diacyl-16:0/22:6) emerged, presumably due to the increase of synthesis or decrease of degradation of PC (diacyl-16:0/22:6).

The present findings indicate that increased levels of PC (diacyl-16:0/22:6) could be a biomarker for neuronal cells of hippocampus CA1 destined to progress to apoptosis, although its exact biochemical role for neuronal cell death is still unknown. One possibility is that the increase of PC (diacyl-16:0/22:6) results from

the decreased degradation of PC (diacyl-16:0/22:6). PC (diacyl-16:0/22:6) is known to contain DHA, a type of polyunsaturated fatty acid, which is freed from PC by phospholipase A_2 and metabolized to provide various mediators with neuroprotective function (Serhan et al., 2006; Eady et al., 2012). Decreased degradation of PC (diacyl-16:0/22:6) might decrease the relative amount of DHA and its anti-apoptotic effect in the neuronal cell and consequently contribute to delayed neuronal cell death. To prove this hypothesis, further molecular biological analysis is required, such as identification of the specific degradation enzyme of PC (diacyl-16:0/22:6) with function inhibited under ischemic stress.

While we focused on dynamics of PC species in neuronal cell death in this study, the brain lipidome is quite diverse, consisting of glycerophospholipids such as phosphatidylethanolamines, phosphatidylinositols, phosphatidylserine, phosphatidylglycerols, cardiolipins, and glycerolipids, mainly triacylglycerols, besides PCs. Therefore we have to admit the possibility that other lipid species besides PC species may show significant changes in the superacute phase of TGI. Visualization of diverse lipid species by IMS would be enabled using appropriate matrix, such as ionized silver particles (Jackson et al., 2014). Coupling of IMS with MALDI-ion mobility mass spectrometry would be also a robust method to allow the separation and detection of a wide range of diverse lipid species (Jackson et al., 2014).

There have been several reports emphasizing the importance that a well-defined sample handling procedure can minimize the time-dependent lipid degradation of the samples prepared for IMS analysis (Patterson et al., 2014; Thomas and Chaurand, 2014). According to the procedure, rat brains were rapidly removed from the skull within a few minutes after euthanasia and frozen in powdered dry ice, and then stored at −80 °C until use. The coronal cryostat sections placed onto glass slides were applied with matrix and subsequent IMS analysis was performed. As the present study dealt with extremely subtle molecular changes associated with TGI, we have paid special attention to minimize such postmortem changes and the time-dependent degradation of PCs in the samples. Then, the protocol applied in the study is likely to provide a state close to the condition of in situ to detect the molecular changes specific with TGI.

The present study demonstrated that IMS can detect subtle molecular changes such as increase of PC (diacyl-16:0/22:6) in the cells of tissue slices while maintaining the neuroanatomical information, so is a powerful method for studying the molecular mechanisms associated with delayed cell death. The applicability and usefulness of IMS for biological research has been increasingly recognized in several different areas (Waki et al., 2014; Yuki et al., 2014). Further development of IMS, such as higher resolution imaging and technical improvement to detect molecules in smaller quantities (Van de Plas et al., 2015; Waki et al., 2015), will allow detection of a wider range of proteins in addition to phospholipids which have important biological functions. Therefore IMS has the potential to achieve further progress in the study of ischemia.

SOURCES OF FUNDING

This work was supported by a Grant-in-Aid for Scientific Research (B) (No. 25293304) to Dr. Saito, a Grant-in-Aid for Scientific Research (B) (No. 25293044) to Dr. Setou, a Grant-in-Aid for Scientific Research (C) (No. 25462206) to Dr. Imai, and a Grant-in-Aid for Young Scientists (B) (No. 15K19949) to Dr. Miyawaki from the Japan Society for the Promotion of Science. This work was also supported by a Project for Creation of Research Platforms and Sharing of Advanced Research Infrastructure (No. 25801) to Dr. Setou.

DISCLOSURES

The authors declare no conflict of interest.

REFERENCES

Abe K, Aoki M, Kawagoe J, Yoshida T, Hattori A, Kogure K, Itoyama Y (1995) Ischemic delayed neuronal death. A mitochondrial hypothesis. Stroke 26:1478–1489.

Adibhatla RM, Hatcher JF, Dempsey RJ (2006) Lipids and lipidomics in brain injury and diseases. AAPS J 8:E314–E321.

Aebersold R, Mann M (2003) Mass spectrometry-based proteomics. Nature 422:198–207.

Andine P, Jacobson I, Hagberg H (1988) Calcium uptake evoked by electrical stimulation is enhanced postischemically and precedes delayed neuronal death in CA1 of rat hippocampus: involvement of N-methyl-D-aspartate receptors. J Cereb Blood Flow Metab 8:799–807.

Asai A, Tanahashi N, Qiu JH, Saito N, Chi S, Kawahara N, Tanaka K, Kirino T (2002) Selective proteasomal dysfunction in the hippocampal CA1 region after transient forebrain ischemia. J Cereb Blood Flow Metab 22:705–710.

Blanco-Suarez E, Fiuza M, Liu X, Chakkarapani E, Hanley JG (2014) Differential Tiam1/Rac1 activation in hippocampal and cortical neurons mediates differential spine shrinkage in response to oxygen/glucose deprivation. J Cereb Blood Flow Metab 34:1898–1906.

Button EB, Mitchell AS, Domingos MM, Chung JH, Bradley RM, Hashemi A, Marvyn PM, Patterson AC, Stark KD, Quadrilatero J, Duncan RE (2014) Microglial cell activation increases saturated and decreases monounsaturated fatty acid content, but both lipid species are proinflammatory. Lipids 49:305–316.

Cornett DS, Reyzer ML, Chaurand P, Caprioli RM (2007) MALDI imaging mass spectrometry: molecular snapshots of biochemical systems. Nat Methods 4:828–833.

Eady TN, Belayev L, Khoutorova L, Atkins KD, Zhang C, Bazan NG (2012) Docosahexaenoic acid signaling modulates cell survival in experimental ischemic stroke penumbra and initiates long-term repair in young and aged rats. PLoS One 7:e46151.

Fenn JB, Mann M, Meng CK, Wong SF, Whitehouse CM (1989) Electrospray ionization for mass spectrometry of large biomolecules. Science 246:64–71.

Gessel MM, Norris JL, Caprioli RM (2014) MALDI imaging mass spectrometry: spatial molecular analysis to enable a new age of discovery. J Proteomics 107:71–82.

Glynn P (2013) Neuronal phospholipid deacylation is essential for axonal and synaptic integrity. Biochim Biophys Acta 1831:633–641.

Goto Y, Okamoto S, Yonekawa Y, Taki W, Kikuchi H, Handa H, Kito M (1988) Degradation of phospholipid molecular species during experimental cerebral ischemia in rats. Stroke 19:728–735.

Goto-Inoue N, Hayasaka T, Zaima N, Setou M (2011) Imaging mass spectrometry for lipidomics. Biochim Biophys Acta 1811:961–969.

Grimm MO, Grösgen S, Riemenschneider M, Tanila H, Grimm HS, Hartmann T (2011) From brain to food: analysis of

phosphatidylcholins, lyso-phosphatidylcholins and phosphatidylcholin–plasmalogens derivates in Alzheimer's disease human post mortem brains and mice model via mass spectrometry. J Chromatogr A 16:14028–14039.
Hanada M, Sugiura Y, Shinjo R, Masaki N, Imagama S, Ishiguro N, Matsuyama Y, Setou M (2012) Spatiotemporal alteration of phospholipids and prostaglandins in a rat model of spinal cord injury. Anal Bioanal Chem 403:1873–1884.
Hankin JA, Farias SE, Barkley RM, Heidenreich K, Frey LC, Hamazaki K, Kim HY, Murphy RC (2011) MALDI mass spectrometric imaging of lipids in rat brain injury models. J Am Soc Mass Spectrom 22:1014–1021.
Hermansson M, Hokynar K, Somerharju P (2011) Mechanisms of glycerophospholipid homeostasis in mammalian cells. Prog Lipid Res 50:240–257.
Jackson SN, Baldwin K, Muller L, Womack VM, Schultz JA, Balaban C, Woods AS (2014) Imaging of lipids in rat heart by MALDI-MS with silver nanoparticles. Anal Bioanal Chem 406:1377–1386.
Jackson SN, Barbacci D, Egan T, Lewis EK, Schultz JA, Woods AS (2014) MALDI-ion mobility mass spectrometry of lipids in negative ion mode. Anal Methods 6:5001–5007.
James R, Searcy JL, Le Bihan T, Martin SF, Gliddon CM, Povey J, Deighton RF, Kerr LE, McCulloch J, Horsburgh K (2012) Proteomic analysis of mitochondria in APOE transgenic mice and in response to an ischemic challenge. J Cereb Blood Flow Metab 32:164–176.
Kawahara N, Ide T, Saito N, Kawai K, Kirino T (1998) Propentofylline potentiates induced ischemic tolerance in gerbil hippocampal neurons via adenosine receptor. J Cereb Blood Flow Metab 18:472–475.
Kawahara N, Wang Y, Mukasa A, Furuya K, Shimizu T, Hamakubo T, Aburatani H, Kodama T, Kirino T (2004) Genome-wide gene expression analysis for induced ischemic tolerance and delayed neuronal death following transient global ischemia in rats. J Cereb Blood Flow Metab 24:212–223.
Kirino T (1982) Delayed neuronal death in the gerbil hippocampus following ischemia. Brain Res 239:57–69.
Koizumi S, Yamamoto S, Hayasaka T, Konishi Y, Yamaguchi-Okada M, Goto-Inoue N, Sugiura Y, Setou M, Namba H (2010) Imaging mass spectrometry revealed the production of lyso-phosphatidylcholine in the injured ischemic rat brain. Neuroscience 168:219–225.
Kubota M, Nakane M, Nakagomi T, Tamura A, Hisaki H, Shimasaki H, Ueta N (2001) Regional distribution of ethanolamine plasmalogen in the hippocampal CA1 and CA3 regions and cerebral cortex of the gerbil. Neurosci Lett 301:175–178.
Nakatomi H, Kuriu T, Okabe S, Yamamoto S, Hatano O, Kawahara N, Tamura A, Kirino T, Nakafuku M (2002) Regeneration of hippocampal pyramidal neurons after ischemic brain injury by recruitment of endogenous neural progenitors. Cell 110:429–441.
Oya S, Yoshikawa G, Takai K, Tanaka JI, Higashiyama S, Saito N, Kirino T, Kawahara N (2009) Attenuation of Notch signaling promotes the differentiation of neural progenitors into neurons in the hippocampal CA1 region after ischemic injury. Neuroscience 158:683–692.
Patterson NH, Thomas A, Chaurand P (2014) Monitoring time-dependent degradation of phospholipids in sectioned tissues by MALDI imaging mass spectrometry. J Mass Spectrom 49:622–627.
Paxinos G, Watson C (2006) The rat brain in stereotaxic coordinates. 6th ed. San Diego, CA: Academic Press.
Pulsinelli WA, Brierley JB, Plum F (1982) Temporal profile of neuronal damage in a model of transient forebrain ischemia. Ann Neurol 11:491–498.
Schmidt-Kastner R, Freund TF (1991) Selective vulnerability of the hippocampus in brain ischemia. Neuroscience 40:599–636.
Serhan CN, Gotlinger K, Hong S, Lu Y, Siegelman J, Baer T, Yang R, Colgan SP, Petasis NA (2006) Anti-inflammatory actions of neuroprotectin D1/protectin D1 and its natural stereoisomers: assignments of dihydroxy-containing docosatrienes. J Immunol 176:1848–1859.
Shanta SR, Choi CS, Lee JH, Shin CY, Kim YJ, Kim KH, Kim KP (2012) Global changes in phospholipids identified by MALDI MS in rats with focal cerebral ischemia. J Lipid Res 53:1823–1831.
Shindou H, Shimizu T (2009) Acyl-CoA:lysophospholipid acyltransferases. J Biol Chem 284:1–5.
Sugiura Y, Konishi Y, Zaima N, Kajihara S, Nakanishi H, Taguchi R, Setou M (2009) Visualization of the cell-selective distribution of PUFA-containing phosphatidylcholines in mouse brain by imaging mass spectrometry. J Lipid Res 50:1776–1788.
Sun GY, Xu J, Jensen MD, Simonyi A (2004) Phospholipase A2 in the central nervous system: implications for neurodegenerative diseases. J Lipid Res 45:205–213.
Suzuki R, Yamaguchi T, Li CL, Klatzo I (1983) The effects of 5-minute ischemia in Mongolian gerbils: II. Changes of spontaneous neuronal activity in cerebral cortex and CA1 sector of hippocampus. Acta Neuropathol 60:217–222.
Thomas A, Chaurand P (2014) Advances in tissue section preparation for MALDI imaging MS. Bioanalysis 6:967–982.
Van de Plas R, Yang J, Spraggins J, Caprioli RM (2015) Image fusion of mass spectrometry and microscopy: a multimodality paradigm for molecular tissue mapping. Nat Methods 12:366–372.
Waki M, Ide Y, Ishizaki I, Nagata Y, Masaki N, Sugiyama E, Kurabe N, Nicolaescu D, Yamazaki F, Hayasaka T, Ikegami K, Kondo T, Shibata K, Hiraide T, Taki Y, Ogura H, Shiiya N, Sanada N, Setou M (2014) Single-cell time-of-flight secondary ion mass spectrometry reveals that human breast cancer stem cells have significantly lower content of palmitoleic acid compared to their counterpart non-stem cancer cells. Biochimie 107:73–77.
Waki M, Sugiyama E, Kondo T, Sano K, Setou M (2015) Nanoparticle-assisted laser desorption/ionization for metabolite imaging. Methods Mol Biol 1203:159–173.
Wang HY, Wu HW, Tsai PJ, Liu CB (2012) MALDI-mass spectrometry imaging of desalted rat brain sections reveals ischemia-mediated changes of lipids. Anal Bioanal Chem 404:113–124.
Yonekura I, Takai K, Asai A, Kawahara N, Kirino T (2006) P53 potentiates hippocampal neuronal death caused by global ischemia. J Cereb Blood Flow Metab 26:1332–1340.
Yuki D, Sugiura Y, Zaima N, Akatsu H, Takei S, Yao I, Maesako M, Kinoshita A, Yamamoto T, Kon R, Sugiyama K, Setou M (2014) DHA-PC and PSD-95 decrease after loss of synaptophysin and before neuronal loss in patients with Alzheimer's disease. Sci Rep 4:7130.

(Accepted 2 February 2016)
(Available online 9 February 2016)